Bioactive Materials 32 (2024) 333–343

Contents lists available at ScienceDirect

Bioactive Materials

journal homepage: www.keaipublishing.com/en/journals/bioactive-materials

On the origin of the low immunogenicity and biosafety of a neutral α-helical polypeptide as an alternative to polyethylene glycol

Jialing Sun [a,1], Junyi Chen [b,1], Yiming Sun [a], Yingqin Hou [a], Zhibo Liu [b,c,**], Hua Lu [a,*]

[a] Beijing National Laboratory for Molecular Sciences, Center for Soft Matter Science and Engineering, Key Laboratory of Polymer Chemistry and Physics of Ministry of Education, College of Chemistry and Molecular Engineering, Peking University, Beijing, 100871, China
[b] Beijing National Laboratory for Molecular Sciences, Radiochemistry and Radiation Chemistry Key Laboratory of Fundamental Science, NMPA Key Laboratory for Research and Evaluation of Radiopharmaceuticals, Key Laboratory of Bioorganic Chemistry and Molecular Engineering of Ministry of Education, College of Chemistry and Molecular Engineering, Peking University, Beijing, 100871, China
[c] Peking University–Tsinghua University Center for Life Sciences, Peking University, Beijing, 100871, China

A B S T R A C T

Poly(ethylene glycol) (PEG) is a prominent synthetic polymer widely used in biomedicine. Despite its notable success, recent clinical evidence highlights concerns regarding the immunogenicity and adverse effects associated with PEG in PEGylated proteins and lipid nanoparticles. Previous studies have found a neutral helical polypeptide poly(γ-(2-(2-(2-methoxyethoxy)ethoxy)ethyl $_{L}$-glutamate), namely $_{L}$-P(EG_3Glu), as a potential alternative to PEG, displaying lower immunogenicity. To comprehensively assess the immunogenicity, distribution, degradation, and biosafety of $_{L}$-P(EG_3Glu), herein, we employ assays including enzyme-linked immunosorbent assay, positron emission tomography-computed tomography, and fluorescent resonance energy transfer. Our investigations involve *in vivo* immune responses, biodistribution, and macrophage activation of interferon (IFN) conjugates tethered with helical $_{L}$-P(EG_3Glu) (L20k-IFN), random-coiled $_{DL}$-P(EG_3Glu) (DL20k-IFN), and PEG (PEG20k-IFN). Key findings encompass: minimal anti-IFN and anti-polymer antibodies elicited by L20k-IFN; length-dependent affinity of PEG to anti-PEG antibodies; accelerated clearance of DL20k-IFN and PEG20k-IFN linked to anti-IFN and anti-polymer IgG; complement activation for DL20k-IFN and PEG20k-IFN but not L20k-IFN; differential clearance with L20k-IFN kidney-based, and DL20k-IFN/PEG20k-IFN accumulation mainly in liver/spleen; enhanced macrophage activation by DL20k-IFN and PEG20k-IFN; $_{L}$-P(EG_3Glu) resistance to proteolysis; and safer repeated administrations of $_{L}$-P(EG_3Glu) in rats. Overall, this study offers comprehensive insights into the lower immunogenicity of $_{L}$-P(EG_3Glu) compared to $_{DL}$-P(EG_3Glu) and PEG, supporting its potential clinical use in protein conjugation and nanomedicines.

1. Introduction

Poly(ethylene glycol) (PEG) is a synthetic polymer widely used for versatile biomedical applications ranging from surface coating, nanoparticle functionalization, protein conjugation (i.e. PEGylation), to vaccine and drug excipients [1–3]. Its remarkable versatility owes much to its highly hydrated and conformationally flexible nature, primarily harnessed for stealth and antifouling purposes. This involves reducing non-specific adsorption, prolonging blood circulation, and mitigating unwanted immune responses. The success of PEG is manifested by the clinical approval of more than a dozen PEGylated drugs, mostly proteins/peptides, and very recently, the COVID-19 mRNA vaccine delivered by the PEG-functionalized lipid nanoparticles (PEG-LNPs) [4–7]. However, amid these commendable accomplishments, the past two decades have witnessed mounting concerns regarding the chronic toxicity and emerging immunogenicity of PEG [8–12]. One significant issue pertains to the accumulation of nondegradable PEG, which has been linked to vacuolization of macrophages and epithelial cells in various tissues, including the kidneys and spleen [13,14]. Additionally, PEG, acting as a hapten, has been shown to induce the production of anti-PEG antibodies when attached to carriers like proteins or LNPs [15]. The presence of these anti-PEG antibodies can lead to mild allergic reactions or even life-threatening anaphylaxis [16–19], and can accelerate the clearance of PEG-containing materials from the bloodstream,

Peer review under responsibility of KeAi Communications Co., Ltd.
* Corresponding author.
** Corresponding author. Beijing National Laboratory for Molecular Sciences, Radiochemistry and Radiation Chemistry Key Laboratory of Fundamental Science, NMPA Key Laboratory for Research and Evaluation of Radiopharmaceuticals, Key Laboratory of Bioorganic Chemistry and Molecular Engineering of Ministry of Education, College of Chemistry and Molecular Engineering, Peking University, Beijin, 100871, China.
E-mail addresses: zbliu@pku.edu.cn (Z. Liu), chemhualu@pku.edu.cn (H. Lu).
[1] J.L.S, and J.Y.C. contributed equally to this work.

https://doi.org/10.1016/j.bioactmat.2023.10.011
Received 12 August 2023; Received in revised form 9 October 2023; Accepted 10 October 2023

known as the "accelerated blood clearance" (ABC) effect [20–23]. A pertinent example is Pegloticase, a heavily PEGylated uricase used in chronic gout treatment, which triggered anti-PEG antibody formation in over 80 % of patients, resulting in a response rate of less than 50 % after repeated administrations [24]. Compounding these concerns is the widespread use of PEG in everyday products such as shampoos, toothpaste, and cosmetics. This has led to the detection of preexisting anti-PEG antibodies in healthy individuals, with the percentage of anti-PEG positive populations rising from under 0.1 % in the 1980s to over 40 % by 2014 [18,25]. An alarming clinical survey has also indicated a strong correlation between increased systemic side effects of COVID-19 LNP-mRNA vaccines and the titers of anti-PEG antibodies, showing a significant increase of 70.9-fold and 377.1-fold for IgG and IgM, respectively [26]. While further research is required to establish the cross-reactivity of these antibodies with other PEGylated products, the urgency and significance of identifying PEG alternatives cannot be understated.

Various synthetic polymers and recombinant biopolymers have emerged as promising substitutes for PEG, achieving varying degrees of success [27–48]. Among them, we focus on synthetic polypeptides (a.k.a. poly(amino acid)s) made by the ring-opening polymerization (ROP) of α-amino acid *N*-carboxyanhydrides (NCA) [49–51]. The appeal of polypeptides lies in their inherent biodegradability and diverse side-chain functionalities. Furthermore, the ability to readily tune their secondary structures adds another layer of versatility [52,53]. Recent strides have been made in developing polypeptides that exhibit superior antifouling properties and reduced immunogenicity compared to PEG. This has been observed in scenarios involving protein-polymer conjugates and bulk hydrogels [54–64]. Notably, the introduction of a neutral α-helical polypeptide, poly(γ-(2-(2-(2-methoxyethoxy)ethoxy)ethyl $_{L}$-glutamate), namely $_{L}$-P(EG_3Glu), for conjugation with human interferon-α2b (IFN) or human growth hormone (GH) resulted in significantly inhibited generation of both anti-protein and anti-polymer antibodies [60,65]. Intriguingly, the analogous random-coiled poly (γ-(2-(2-(2-methoxyethoxy)ethoxy)ethyl $_{DL}$-glutamate) ($_{DL}$-P(EG_3Glu)), possessing the same side chain and an equivalent number-average molar mass (M_n), failed to confer the same degree of immunogenicity mitigation as the helical $_{L}$-P(EG_3Glu).

However, the immunogenicity of polypeptides with distinct secondary structures has yielded inconclusive and sometimes controversial outcomes. Early studies suggested that left-handed helical polypeptides constructed from $_{D}$-configurated glutamate, alanine, and tyrosine were less immunogenic compared to their enantiomeric counterparts composed of $_{L}$-amino acids [66]. Some researchers attributed the diminished immunogenicity of these $_{D}$-polypeptides to the absence of an *in vivo* proteolytic degradation mechanism [67]. Conjugation of $_{DL}$-polyalanine was reported to improve pharmacokinetics and reduce immunogenicity of asparaginase, but antibodies against $_{DL}$-polyalanine were not examined [68]. Conversely, conflicting findings have been reported, with antiserum of $_{DL}$-polyalanine-BSA conjugates reportedly recognizing $_{D}$-polyalanine but not $_{L}$-polyalanine [69]. More recently, implants based on $_{DL}$-polyserine were found low immunogenic and evoked minimal foreign body reactions (FBR) [70]. Given these discrepancies, rigorous experimental investigations with well-designed control groups are imperative to offer fresh insights into the immunogenicity of polypeptide secondary structures and chirality.

In this study, a series of site-specific polymer-IFN conjugates serve as a model system to delve into the underlying causes of the mitigated immunogenicity effects observed with helical $_{L}$-P(EG_3Glu) in comparison to the unstructured $_{DL}$-P(EG_3Glu) and PEG. To achieve this, multiple -terminal specific IFN conjugates were prepared, utilizing $_{L}$-P(EG_3Glu) (L5k-IFN, L20k-IFN, L40k-IFN, and L80k-IFN), $_{D}$-P(EG_3Glu) (D20k-IFN), $_{DL}$-P(EG_3Glu) (DL20k-IFN), and PEG (PEG20k-IFN) (Fig. 1A), where the numerical descriptors represent the M_n of the polymers in Daltons. An integrated approach encompassing enzyme linked immunosorbent assay (ELISA), flow cytometry, and positron emission tomography-computed tomography (PET-CT) was adopted to comprehensively examine immunogenicity, pharmacokinetics, distribution, macrophage uptake, and complement activation behaviors of these conjugates. Concurrently, the *in vitro* and *in vivo* degradation of $_{L}$-/$_{DL}$-P(EG_3Glu) were probed using size exclusion chromatography (SEC) and fluorescent resonance energy transfer (FRET). Finally, the repeat-dose toxicity of $_{L}$-P(EG_3Glu) and PEG were meticulously evaluated and subjected to close comparison.

2. Results

2.1. L20k-IFN and D20k-IFN provoked less anti-drug antibodies than DL20k-IFN and PEG20k-IFN

L20k-IFN, D20k-IFN, DL20k-IFN, and PEG20k-IFN were prepared by the chemoselective native chemical ligation (NCL) (Fig. S1) and characterized with sodium dodecyl sulfate-polyacrylamide gel electrophoresis (SDS-PAGE) and circular dichroism (CD) spectroscopy (Fig. 1B and C) [60,72]. SD rats were subcutaneously (s. c.) immunized with the conjugates for four times at a weekly frequency and the antisera were drawn 7 days after each immunization for the analysis of anti-IFN/anti-polymer antibodies (Fig. 1D, Fig. S2). It was found that anti-IFN IgM and IgG titers in the antisera of L20k-IFN on day 28 (week 4) were 11–41 fold lower than those of DL20k-IFN and PEG20k-IFN antisera (Fig. 1E and F). Interestingly, the levels of anti-IFN IgM and IgG in the D20k-IFN antisera were similarly low to that of the L20k-IFN antisera (Fig. 1E and F). As far as anti-polymer IgM and IgG were concerned, the L20k-IFN antisera were again the lowest among all four conjugates (Fig. 1G and H). For instance, the anti-polymer IgM titers of the L20k-IFN antisera were 81 and 163 times lower than that of DL20k-IFN and PEG20k-IFN, respectively (Fig. 1G). D20k-IFN appeared to elicit more anti-polymer IgM than L20k-IFN, but to a less degree than DL20k-IFN did. To study the size-dependent immunogenicity of $_{L}$-P(EG_3Glu), we generated analogous conjugates of different sizes, namely L5k-IFN, L20k-IFN, L40k-IFN, and L80k-IFN [73] by NCL (Fig. S3) for immunization. While the cellular activity and elimination half-lives ($t_{1/2\beta}$) of these conjugates with $_{L}$-P(EG_3Glu) showed characteristic size-dependence (Fig. S4), interestingly, no significant difference on the levels of anti-IFN and anti-polymer antibodies was observed in these antisera (Fig. S5).

To gain information on the recognition motifs of the anti-polymer antibodies, we conducted competitive ELISA by using a pool of selected competing reagents (Fig. 2A). Presumably, the reagents with the strongest competing ability would most likely resemble the epitope structure recognizing by the antibody. Here, oligoethylene glycol (EG) of different lengths and/or terminal groups were used to analyze the possible epitopes of anti-PEG antibodies (Fig. 2A). It was found that the length (or degree of polymerization, DP), rather than the terminal group, of the competing agents was the primary factor determining the competition ability. Briefly, neither EG_3 nor mEG_3 exhibited significant binding ability to anti-PEG IgG and IgM until reaching an exceedingly high concentration of 1.0 mg/mL (Fig. 2B and C). Competitors with a DP of six or larger (EG_6, EG_{22}, PEG20k, and mPEG20k) all displayed strong binding to anti-PEG IgG and IgM, regardless of the terminal group being a hydroxyl or methoxyl group (Fig. 2B and C). For the anti-DL20k antibodies, it was found that they bind the monomeric $_{D}$-EG_3-Glu stronger than $_{L}$-EG_3-Glu (Fig. 2D and E). Among the three polymeric competitors, L20k and DL20k displayed the weakest and strongest binding to anti-DL20k antibodies, respectively (Fig. 2D and E).

2.2. DL20k-IFN and PEG20k-IFN activated complement system upon the initial exposure only and anti-drug antibodies were responsible for the ABC effect

To study the ABC effect upon repeated injections, antisera at designated time points were collected after the 1st and 3rd immunizations (Fig. 3A, ABC groups). The area under curve ($AUC_{0.5–36h}$) of L20k-IFN

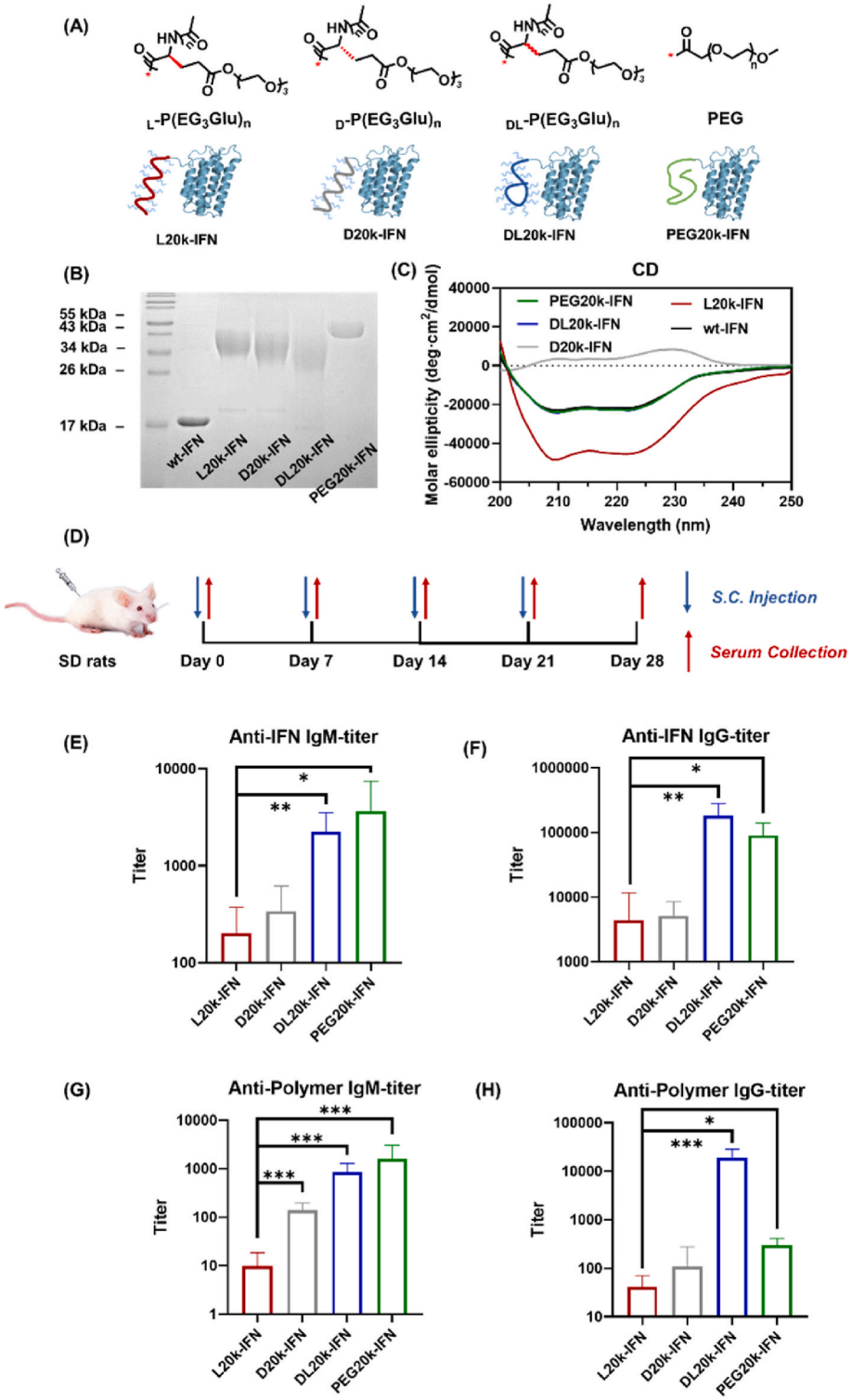

Fig. 1. L20k-IFN is consistently less immunogenic than DL20k-IFN and **PEG20k-IFN.** (A) Structure of the polymers used for IFN conjugation and cartoon illustration of the corresponding IFN conjugates highlighting the differences in polymer conformations. (B–C) 15 % SDS-PAGE (B) and CD spectra (C) of wild-type IFN (wt-IFN) and various polymer-IFN conjugates. (D) Scheme of the immunization regimen and antiserum collection schedule: Female SD rats ($n = 5$) were s. c. injected with L20k-IFN, D20k-IFN, DL20k-IFN, or PEG20k-IFN at a weekly dose 0.2 mg IFN/kg for 4 weeks; antisera were drawn every week starting from day 0. (E–H) The titers of anti-IFN IgM (E), anti-IFN IgG (F), anti-polymer IgM (G), and anti-polymer IgG (H) on day 28. ELISA protocol: for anti-IFN antibody detection, the ELISA plates were coated with wt-IFN; for each polymer-of-interest, the ELISA plates were coated with the corresponding polymer-eGFP conjugates [71]. After coating, antisera were diluted to a series of concentrations and added into the plates. The antisera were incubated in the plates at room temperature for 1 h. After washing, all plates were incubated with anti-rat IgG-HRP or IgM-HRP, and colored with TMB solution (CWBIO). The antibody titer was determined as the maximal diluted factor with a signal/noise over 2. For all the anti-polymer antibody measurements, Tween-20 was replaced with 3-((3-cholamidopropyl) dimethylammonium)-1-propanesulfonate (CHAPS). Data are expressed as mean ± SD ($n = 5$). *P* values are determined by *t*-test analysis: $^{*}P < 0.05$, $^{**}P < 0.01$, $^{***}P < 0.001$.

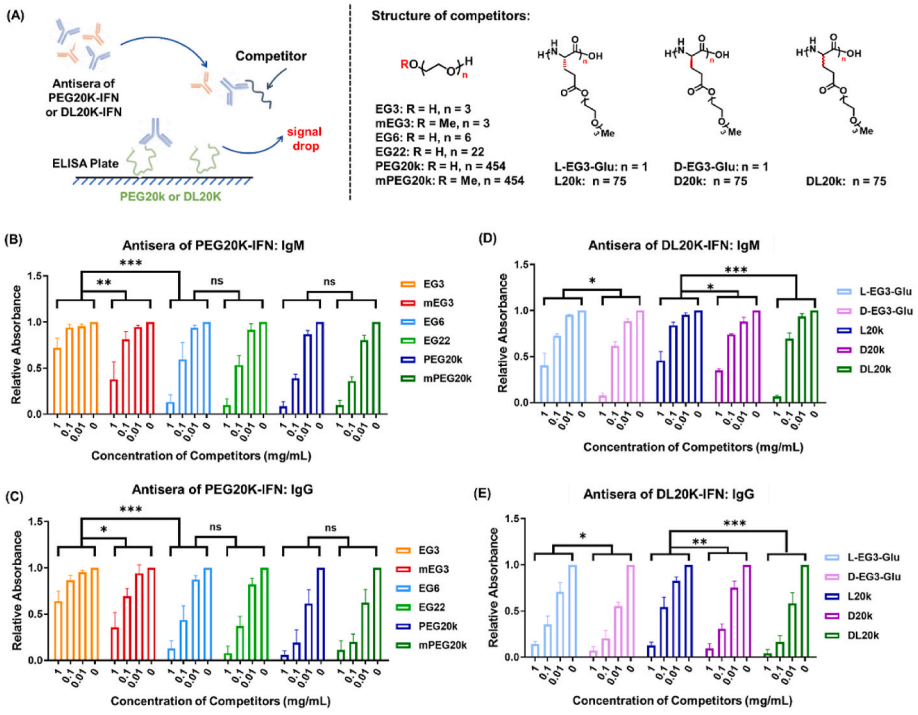

Fig. 2. Competitive ELISA revealed information on the recognition motifs of anti-PEG and anti-DL20k antibodies. (A) Schematic illustration of the principle of the competitive ELISA and structure of competitors. In brief, the ELISA plates were coated with either PEG20k-eGFP or DL20k-eGFP to bind anti-PEG or anti-DL20k antibodies in the antisera, respectively. Antisera were diluted with buffers containing selected competing reagents for incubation. After washing, all plates were incubated with anti-rat IgG-HRP or IgM-HRP, and colored with TMB solution (CWBIO). (B–C) Concentration-dependent changes of anti-PEG (B) IgM and (C) IgG ELSIA signals with various competitors. (D–E) Concentration-dependent changes of anti-DL20k (D) IgM and (E) IgG ELSIA signals with the addition of various competitors. Data are expressed as mean ± SD (n = 5). *P* values are determined by two-way ANOVA (Bonferroni post-test) analysis: $^{*}P < 0.05$, $^{**}P < 0.01$, $^{***}P < 0.001$.

after the 1st and 3rd dose were comparable, suggesting no ABC effect. However, the $AUC_{0.5–36h}$ of DL20k-IFN and PEG20k-IFN after the 3rd injection were only ~26 % and 32 % relative to their 1st injections (Fig. 3B and Fig. S6), respectively, a clear indication of ABC effect.

Previous studies have suggested complement activation upon injection of PEGylated LNPs [9]. For this, we measured the contents of sc5b-9, the terminal complement complex mutually shared by all three pathways of complement activation. L20k-IFN displayed no detectable elevation of sc5b-9, while both DL20k-IFN and PEG20k-IFN boosted the concentration of sc5b-9 at 0.5 h but not 3 h after the 1st injection (Fig. 3C). In the 3rd injection, however, sc5b-9 levels were unchanged at both 0.5 and 3 h for all groups (Fig. 3D).

The ABC effect of PEGylated subjects was previously attributed to antidrug antibodies but very little is known about which type(s) of antibodies were most responsible for the rapid elimination. For this, the dynamic changes of the relative antibody contents in the antisera of DL20k-IFN and PEG20k-IFN before (0 h) and after (0.5, 3, 9, 12 h, 24 h and 36 h) the 3rd injection were examined. For both conjugates, the ABC groups were compared with the control groups receiving only two immunizations (control group, Fig. 3A), which gave essentially flat or slow-declining "baseline" profiles of the antibody contents 7 days after the 2nd immunizations. In contrast, significant declines in the contents of anti-IFN and anti-polymer IgM and IgG were clearly seen over the post 0–36 h upon the 3rd injection of DL20k-IFN, with the anti-DL20k IgG exhibiting the steepest drop (Fig. 3E–H). For PEG20k-IFN after the 3rd injection, anti-IFN IgG (Fig. 3J) and anti-PEG IgG (Fig. 3L), but not the anti-IFN IgM (Fig. 3I) in the antisera displayed significant decreases. It should be mention that the content of anti-PEG IgM (Fig. 3K) first experienced an immediate spike at 0.5 h and then followed by the successive slow elimination over the next 36 h, and the underlying reason was still under investigation.

2.3. L20k-IFN was primarily cleared from kidneys, whereas DL20k-IFN and PEG20k-IFN accumulated mainly in liver and spleen

The pharmacokinetics and biodistribution of L20k-IFN, DL20k-IFN, and PEG20k-IFN were investigated via PET-CT imaging. The conjugates were labelled with zirconium-89 (^{89}Zr), a positron-emitting radionuclide with a half-life of 78.4 h, using *p*-isothiocyanato-benzyl-desferrioxamine (DFO) as a bifunctional chelator (Fig. S7). The ^{89}Zr-labelled conjugates, namely ^{89}Zr-L20k-IFN, ^{89}Zr-DL20k-IFN, and ^{89}Zr-PEG20k-IFN were injected into BALB/c mice via the tail vein route. The following PET imaging indicated that the three conjugates were primarily distributed in the blood, liver, and kidneys post injections (Fig. 4A). ^{89}Zr-L20k-IFN mainly cleared from circulation through renal system, and rapidly passed through the renal cortex to the renal medulla near the ureter (zoom-in of Fig. 4A). In contrast, ^{89}Zr-DL20k-IFN and ^{89}Zr-PEG20k-IFN mainly cleared from the blood through the hepatobiliary system, while showing less kidney accumulation.

Time-activity curves (TAC) of heart/blood, liver, and kidneys were drawn according to the radioactive signals of region-of-interest (ROI) in PET imaging (Fig. 4B–D). Of note, due to the small thickness of spleen and the high radioactivity in liver and kidneys, outlining the spleen to calculate the spleen signal was not practical. The elimination half-lives ($t_{1/2\beta}$) of ^{89}Zr-L20k-IFN, ^{89}Zr-DL20k-IFN, and ^{89}Zr-PEG20k-IFN were calculated based on the TAC of heart/blood and determined as 8.4 ± 1.6, 4.4 ± 1.2, and 10.1 ± 0.9 h, respectively (Fig. 4B). The $t_{1/2\beta}$ trend of different conjugates generally agreed well with our previous reported results based on ELISA [60]. No statistical significance ($P = 0.108$) was found for the $t_{1/2\beta}$ of ^{89}Zr-L20k-IFN and ^{89}Zr-PEG20k-IFN (Fig. 4B). TACs of the liver revealed that ^{89}Zr-DL20k-IFN has notably higher liver uptake than those of both ^{89}Zr-L20k-IFN and ^{89}Zr-PEG20k-IFN ($P^{***}<0.0001$, Fig. 4C). This rapid and high accumulation of ^{89}Zr-DL20k-IFN in the liver substantially lowered its concentration in

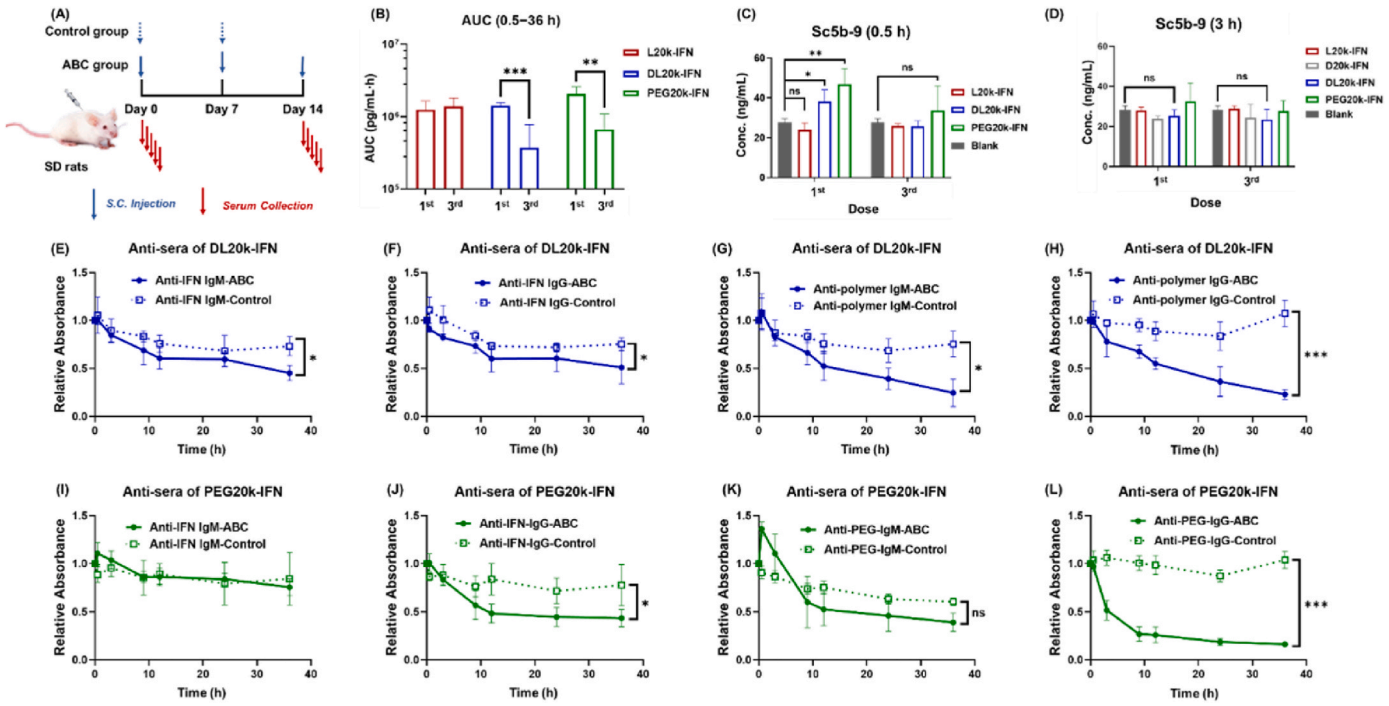

Fig. 3. ABC effect of DL20k-IFN and PEG20k-IFN. (A) Scheme of the immunization regimen and serum collection schedule for the ABC groups and control groups. Female SD rats were s. c. injected with various conjugates for 2 (control groups, $n = 5$ for each group) or 3 (ABC groups, $n = 5$ for each group) times at a weekly dose of 0.2 mg/kg; sera were drawn from the rats at selected time points after the 1st (day 0) and 3rd (day 14) doses. (B) Comparison of the $AUC_{0.5–36h}$ of the 1st and 3rd doses of each IFN conjugate (ABC group). (C–D) Sc5b-9 contents in the antisera (C) 0.5 h and (D) 3 h after the 1st and 3rd immunizations (ABC group), respectively. (E–L) The dynamic change of the relative contents of anti-IFN and anti-polymer antibodies after the 3rd injection of (E–H) DL-20 k-IFN or (I–L) PEG20k-IFN in the antisera of the ABC groups, as compared with those in the control groups (receiving only two injections). Data are expressed as mean ± SD ($n = 5$). P values are determined by t-test analysis for Fig. 3B–D or two-way ANOVA (Bonferroni post-test) analysis for Fig. 3E–L: $^{*}P < 0.05$, $^{**}P < 0.01$, $^{***}P < 0.001$.

the blood, leading to a shorter $t_{1/2\beta}$ than those of the other two conjugates (Fig. 4B, $P = 0.0063$ for ^{89}Zr-PEG20k-IFN, and 0.0003 for ^{89}Zr-L20k-IFN). The kidney uptake of ^{89}Zr-L20k-IFN was significantly higher than those of ^{89}Zr-DL20k-IFN and ^{89}Zr-PEG20k-IFN ($P^{***}<0.0001$). The signal of ^{89}Zr-L20k-IFN in the kidneys reached the apex at about 9 h post the injection, then gradually declined in the following 87 h (Fig. 4D). Different from ^{89}Zr-L20k-IFN, ^{89}Zr-PEG20-k-IFN showed a slow accumulation trend in the kidneys, which may be related to its greater hydrodynamic size (Fig. S8).

Following PET-CT scans, the mice were sacrificed 124 h post injection to collect major organs for radioactivity measurement to characterize the accumulation of the conjugates in specific tissues (Fig. 4E). In consistent with the PET-CT images, ^{89}Zr-DL20k-IFN and ^{89}Zr-PEG20k-IFN were found to accumulate 110 % and 85.8 % injected dose per gram (ID/g) of the liver, whereas ^{89}Zr-L20k-IFN was merely 33.6 % ID/g ($P^{***} = 0.0002$). Interestingly, ^{89}Zr-DL20k-IFN and ^{89}Zr-PEG20k-IFN were found to accumulate also in spleen at a significantly higher level than ^{89}Zr-L20k-IFN ($P^{***} = 0.0008$), with ^{89}Zr-PEG20k-IFN reached 100 % ID/g, the highest among the three conjugates studied.

2.4. L20k-IFN was less internalized by macrophages as compared with DL20k-IFN and PEG20k-IFN

Macrophages were known to play important roles in PEG immunogenicity [9]. To examine the interaction of the conjugates with macrophages, L20k-IFN, DL20k-IFN, and PEG20k-IFN were site-specifically labelled with a red-fluorescent dye Cy5 via the thiol-maleimide chemistry, and incubated with mouse macrophages RAW264.7 *in vitro*. Flow cytometry analysis showed the least internalization of L20k-IFN by RAW264.7 (Fig. 5A and Fig. S9). Furthermore, incubation of L20k-IFN with RAW264.7 stimulated undetectable interleukin-6 (IL-6) and low levels of tumor necrosis factor-α (TNF-α) in the cell medium, ~8 and 7.5-fold lower as compared to those found for DL20k-IFN or PEG20k-IFN (Fig. 5B and C).

2.5. $_{L}$-P(EG$_3$Glu) was more resistant to proteolytic digestion than $_{DL}$-P(EG$_3$Glu) in vitro and in vivo

The degradability of polypeptides may play a role in determining the biodistribution and immunogenicity. For this, the degradation of $_{L}$-P(EG$_3$Glu) and $_{DL}$-P(EG$_3$Glu) under different *in vitro* and *in vivo* conditions were investigated based on the principle of FRET. To ensure a satisfactory FRET signal, 10 kDa instead of 20 kDa was selected for both polypeptides. As shown in Fig. 6A, the *N*- and *C*-termini of two polypeptides were labelled with Cy5 and Cy5.5, which were termed as Cy5-L10k-Cy5.5 and Cy5-DL10k-Cy5.5, respectively (Fig. S10). The *in vitro* proteolytic degradation ratio of Cy5-L10k-Cy5.5 in fresh mouse serum, which can be revealed from the reduction in FRET efficiency (formula provided in Fig. 6A), was found to be ~5 % after 120 h incubation at 37 °C, whereas ~15 % degradation was detected for Cy5-DL10k-Cy5.5 under the same condition (Fig. 6B). The slower degradation of Cy5-L10k-Cy5.5 was also observed in milieu extracted from the lysosomes of RAW264.7 cells (Fig. 6C). To understand this degradation result, the solvent exposure level of the peptide bonds of $_{DL}$- and $_{L}$-P(EG$_3$Glu) was measured with ^{1}H NMR spectroscopy. By dissolving $_{DL}$-P(EG$_3$Glu) and $_{L}$-P(EG$_3$Glu) into D_2O, ^{1}H NMR spectroscopy gave a considerably faster H-D exchange rate of the peptide amide hydrogen (N–H) for the racemic polypeptide over the enantiomeric pure polypeptide (Fig. 6D), suggesting greater solvent-exposure of the backbone for $_{DL}$-P(EG$_3$Glu).

Next, Cy5-L10k-Cy5.5 and Cy5-DL10k-Cy5.5 were intravenously injected into healthy BALB/c mice to examine their degradation *in vivo*. The fluorescence of both polymers was almost undetectable in the serum soon after the injection, and thus unable to determine their half-life. After sacrificing the mice to collect organs at different time points

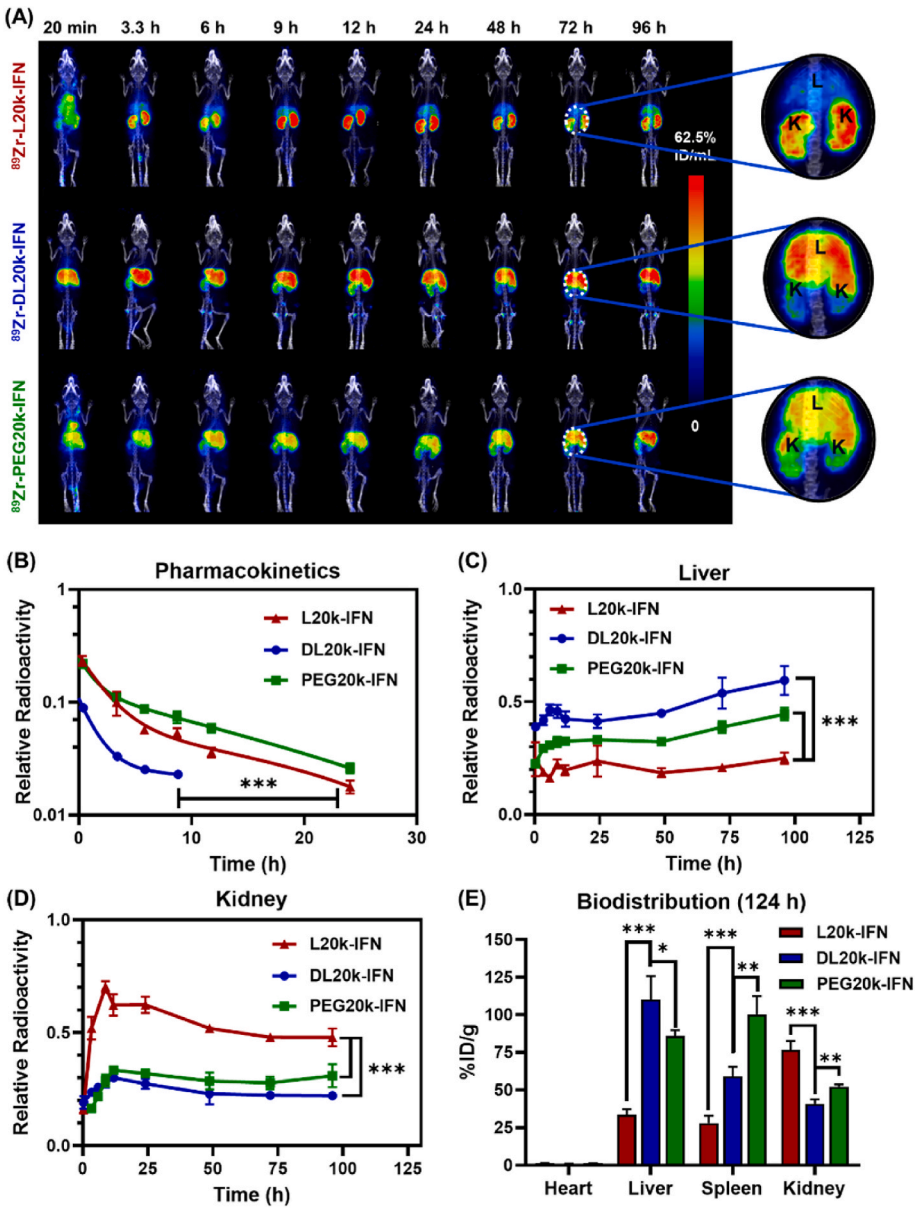

Fig. 4. Biodistribution of L20k-IFN, DL20k-IFN, and PEG20k-IFN revealed by PET-CT imaging and radioactivity measurement. (A) *In vivo* PET-CT images at different time points post injections. Zoom-in photos are the representative regions showing the signals of liver and kidneys 72 h post injection. (B–D) Time-lapsed radioactive signals in different organs (B: heart; C: liver; D: kidney). (E) Relative radio activities normalized with the weight of organs at 124 h post injections of the conjugates. The ^{89}Zr-labelled conjugates were injected into BALB/c mice ($n = 4$) via the tail vein. Data are expressed as mean ± SD ($n = 4$). *P* values are determined by two-way ANOVA (Bonferroni post-test) analysis for Fig. 4B–D or *t*-test analysis for Fig. 4E: $^{*}P < 0.05$, $^{**}P < 0.01$, $^{***}P < 0.001$.

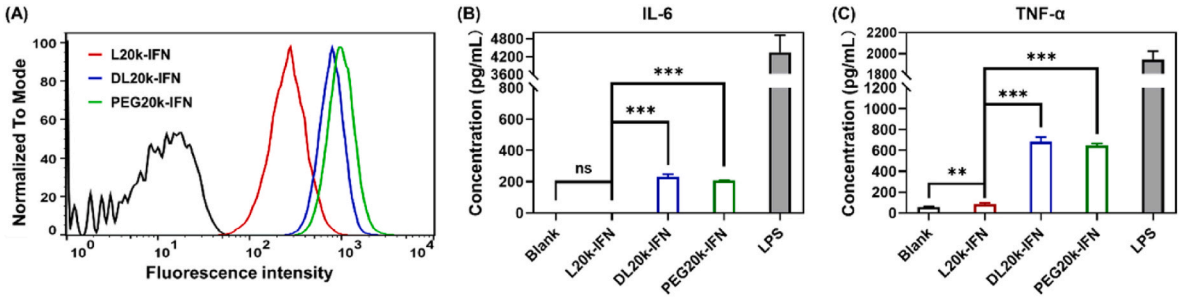

Fig. 5. Macrophage uptake and stimulation of Cy5-labelled conjugates *in vitro*. (A) *In vitro* macrophage (RAW264.7) uptake of Cy5-labelled conjugates characterized by flow cytometry. (B–C) *In vitro* macrophage (RAW264.7) activation by measuring the secretion of (B) IL-6 and (C) TNF-α. Data are expressed as mean ± SD ($n = 3$). *P* values are determined by *t*-test analysis: $^{*}P < 0.05$, $^{**}P < 0.01$, $^{***}P < 0.001$.

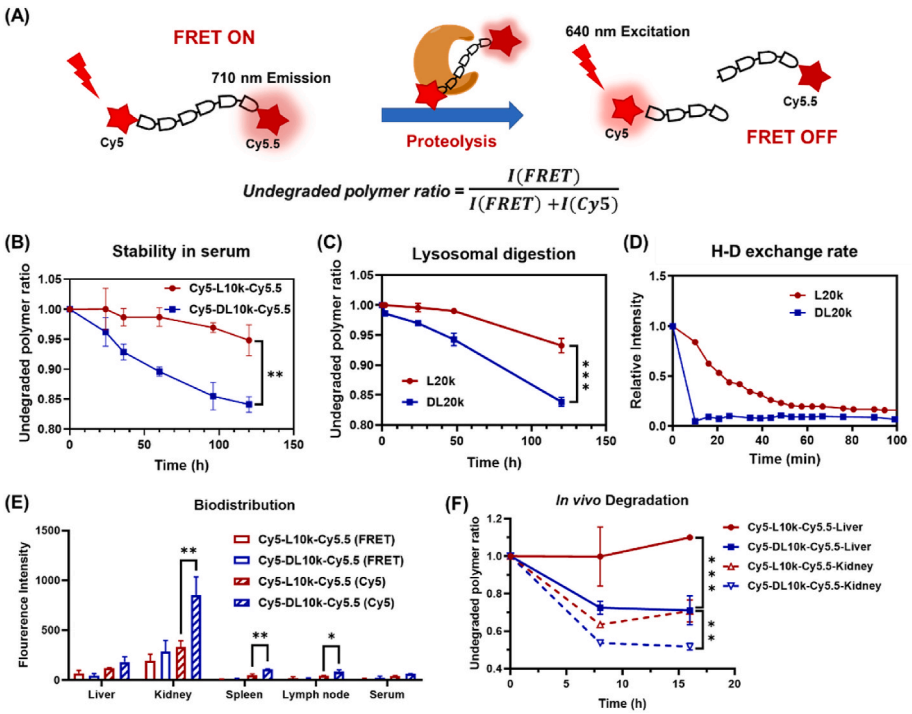

Fig. 6. Degradation and clearance of $_{L}$-P(EG$_3$Glu) and $_{DL}$-P(EG$_3$Glu) *in vivo* and *in vitro*. (A) Schematic illustration of polymer degradation monitored with changes of FRET efficiency. (B–C) *In vitro* degradation ratios of Cy5-L10k-Cy5.5 and Cy5-DL10k-Cy5.5 in (B) fresh mouse serum and (C) extracted lysosome milieu of RAW 264.7 cells. (D) Characterization of the hydrogen-deuterium exchange rates of the backbone N–H of L20k and DL20k using ^{1}H NMR spectroscopy. (E) *In vivo* distribution of Cy5-L10k-Cy5.5 and Cy5-DL10k-Cy5.5 in the major organs 12 h after injection ($n = 3$ for each group). (F) *In vivo* degradation kinetics of Cy5-L10k-Cy5.5 and Cy5-DL10k-Cy5.5 in the liver and kidneys, respectively. BALB/c mice ($n = 3$ for each group) were injected with in the tail vein; after 8 or 16 h, the liver and kidneys were extracted, and homogenized with ultrasonication and lysis; the Cy5 and Cy5.5 fluorescence signal of the tissue extracts was detected with a microplate reader to calculate the FRET efficiency. (FRET channel: excitation at 640 nm, emission at 710 nm; Cy5 channel: excitation at 640 nm, emission at 680 nm; Cy5.5 channel: excitation at 670 nm, emission at 710 nm). Data are expressed as mean ± SD ($n = 3$). *P* values are determined by two-way ANOVA (Bonferroni post-test) analysis for B, C, and F or *t*-test analysis for E: $^*P < 0.05$, $^{**}P < 0.01$, $^{***}P < 0.001$.

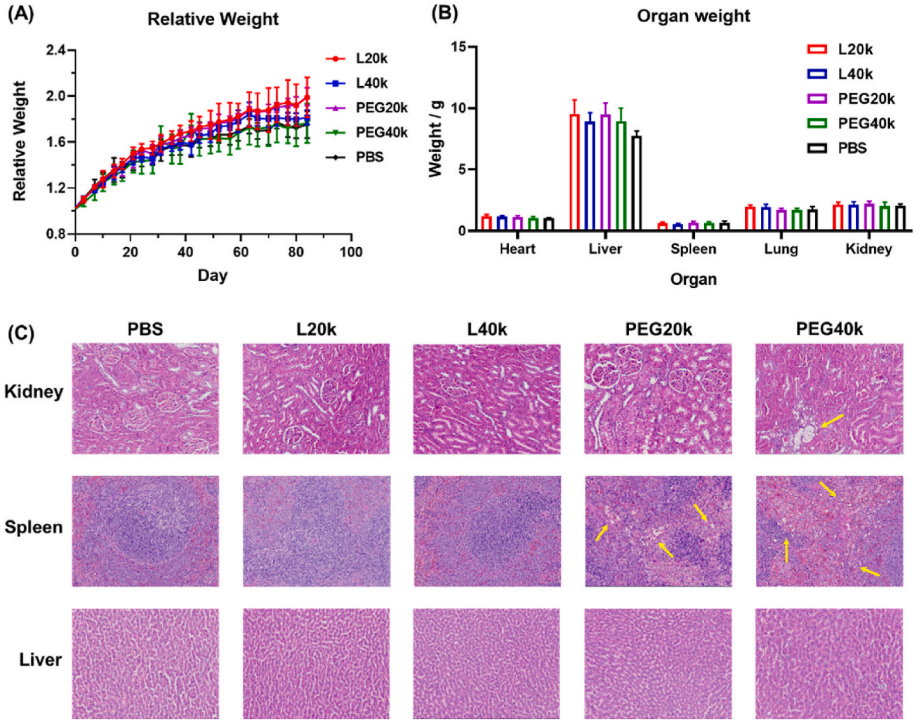

Fig. 7. Repeat-dose toxicity of $_{L}$-P(EG$_3$Glu) and PEG. (A) Change of body weight over 12 weeks for the rats receiving PBS, $_{L}$-P(EG$_3$Glu), or PEG. (B–C) Comparison of (B) body weights and (C) H&E-stained sections of major organs of the rats receiving PBS, $_{L}$-P(EG$_3$Glu), or PEG for 12 weeks. PBS, $_{L}$-P(EG$_3$Glu), or PEG with different M_n were injected into SD rats via the tail vein at a weekly dose of 200 mg/kg repeating for 12 weeks. Data are expressed as mean ± SD (n = 4).

after administration, the remaining polymers were found to majorly accumulate in kidneys and liver as indicated by both the FRET and Cy5 signals in the tissue extracts (Fig. 6E and S11). The overall Cy5.5 and Cy5 intensities of L10k in the liver and kidneys were lower than those of DL10k, suggesting a faster *in vivo* clearance of Cy5-L10k-Cy5.5. The FRET efficiency of Cy5-L10k-Cy5.5 in the homogenized tissue extracts was higher than that of Cy5-DL10k-Cy5.5 group (Fig. 6F), echoing the previous *in vitro* finding of slower degradation of $_{L}$-P(EG_3Glu) than $_{DL}$-P(EG_3Glu). Both polymers showed greater degradation in the kidneys than in the liver as implied by the FRET efficiency (Fig. 6F).

2.6. *$_{L}$-P(EG_3Glu) was less toxic than PEG after repeated doses*

The repeat-dose toxicity of $_{L}$-P$(EG_3Glu)_n$ and PEG was examined in SD rats. Briefly, PBS, $_{L}$-P$(EG_3Glu)_n$ and mPEG of 20 and 40 kDa (termed as L20k, L40k, PEG20k, and PEG40k, respectively) were individually injected into SD rats via the tail vein at a weekly dose of 200 mg/kg for totally 12 weeks. No death nor significant differences in body weight were observed for all groups throughout the entire period of study (Fig. 7A). Examination on the organ weights and blood biochemical indexes showed no sign of liver or kidney dysfunction for rats receiving either $_{L}$-P$(EG_3Glu)_n$ or PEG one week after the last administration (Fig. 7B and S12). Immunohistochemistry of the hematoxylin-eosin (H&E)-stained sections of major organs, however, indicated that PEG20k and PEG40k caused significant vacuolation in the kidneys and spleen (Fig. 7C), which has been well-documented in both literatures [13,30]. In contrast, no organ damages were found for both L20k and L40k.

3. Discussion

In line with the FDA's 2014 guideline on "Immunogenicity Assessment for Therapeutic Protein Products," concerns about PEG immunogenicity intensified following the emergency use authorization of COVID-19 PEG-LNP/mRNA vaccines [16]. The widespread use of these vaccines has raised awareness of PEG immunogenicity, particularly in relation to potential cross-reactivity with preexisting, or boosted anti-PEG antibodies. Notably, failures like pegnivacogen's Phase 3 trial due to severe allergic reactions linked to preexisting anti-PEG antibodies [18,74], and the substantial difference in PEG dose between PEGylated proteins and PEG-LNP/mRNA vaccines (Krystexxa® for example, is ~200 times to that in the PEG-LNP/mRNA vaccine) [75,76], have fueled these concerns.

Past studies suggested initial immune responses to PEGylated substances primarily occurred in the spleen, generating anti-PEG IgM [9,20]. Subsequent repeated injections led to anti-PEG IgM binding to PEGylated objects, triggering complement activation and Kupffer cell (macrophage) engulfment in the liver. Usually, macrophages release cytokines to activate dendritic cells, promote antigen presentation, and recruit T cells to trigger adaptive immune responses. At this stage, the subtype of anti-PEG antibodies typically switches from IgM to IgG in a T-cell dependent manner. Notably, potential antibody-independent complement activation pathways have also been hypothesized, possibly contributing to hypersensitivity reactions [19].

Our findings showed that PEG20k-IFN was predominantly cleared through the liver and strongly accumulated in the spleen (Fig. 4). The *in vitro* uptake of PEG20k-IFN by RAW264.7 cells and subsequent secretion of proinflammatory cytokines such as IL6 and TNFα suggested an important role of macrophages on the origin of PEG immunogenicity (Fig. 5). Notably, IgM-independent complement activation by PEG20k-IFN occurred primarily during the first exposure, similar to the first-dose complement activation in clinical studies of pegnivacogen [18]. On the role of different antibody isotypes on the ABC effect, while Mima et al. emphasized the contribution of anti-PEG IgM [77], our results and other (pre)clinical studies argued anti-PEG IgG [18,76,78]. For this seeming "discrepancy", the timing of examination might matter: Mima et al. examined the ABC effect in the second injection [77], at which point only anti-PEG IgM was presented whereas anti-PEG IgG was yet to be produced; we examined the ABC effect in the third injection when both anti-IFN and anti-PEG IgG were largely generated.

DL20k-IFN showed distribution, clearance patterns, macrophage uptake, and ABC effect largely similar to PEG20k-IFN, suggesting shared elimination pathways and immune response mechanisms (Fig. 4). In contrast, L20k-IFN exhibited distinct distribution due to its smaller hydrodynamic size (Fig. S8), resulting from the folded helical conformation of $_{L}$-P(EG_3Glu). This slow but predominant renal clearance route of L20k-IFN, rather than rapid liver and spleen accumulation (Fig. 8A), leading to lower immunogenicity and prolonged half-life.

Surprisingly, $_{L}$-P(EG_3Glu) exhibited slower degradation than $_{DL}$-P(EG_3Glu), possibly due to its highly folded conformation and dense side groups (Fig. 6). This feature likely provided proteolytic stability for long circulation (Fig. 4A) and minimized immune system attacks by inhibiting antigen digestion, processing, and presenting [67,79]. Once L20K was detached from L20K-IFN, the folded helical conformation and stealthy ability of L20K allowed for quicker clearance as a whole rather than fragments out of the body (Fig. 6E). In contrast, the flexible conformation and quicker degradation of $_{DL}$-P(EG_3Glu) produced antigenic peptidic fragments, stimulating a strong immune response (Fig. 8B). The number of repeating units of EG appeared to be critical as similar length-dependent immunogenicity of EG side chains was previously reported by Chilkoti group [31]. $_{L}$-P(EG_3Glu)'s intrinsic biocompatibility also contributed to its lower immunogenicity and reduced toxicity compared to PEG during prolonged administrations (Fig. 7).

4. Conclusions

In summary, our findings highlight the exceptional biocompatibility of $_{L}$-P(EG_3Glu), rendering it nearly "invisible" to the immune system's response, including complement proteins, macrophages, spleen, and liver interactions. As a result, protein conjugates utilizing $_{L}$-P(EG_3Glu) exhibit remarkably low immunogenicity. In comparison to conventional PEG, $_{L}$-P(EG_3Glu) demonstrates reduced immunogenicity due to the compact EG_3 side chains forming an effective stealth outer layer, while being too short to elicit anti-PEG antibodies. Moreover, when compared to $_{DL}$-P(EG_3Glu), the improved proteolytic stability of $_{L}$-P(EG_3Glu) contributes to prolonged circulation of L20K-IFN in the bloodstream, minimizing premature exposure of antigenic fragments to the immune system. Although the helical conformation of $_{L}$-P(EG_3Glu) renders the polymer and related protein conjugates with relatively smaller hydrodynamic sizes, a seemingly unfavorable parameter, it in fact gives rise to intermediate renal clearance rate, and consequently, higher safety and lower immunogenicity. Furthermore, our research indicates that both anti-IFN and anti-PEG IgG antibodies play a more significant role in the ABC phenomenon of PEG20k-IFN compared to the IgM isotypes. This comprehensive study provides robust nonclinical evidence, firmly endorsing the utilization of $_{L}$-P(EG_3Glu) for protein conjugation purposes. We are optimistic that $_{L}$-P(EG_3Glu) holds substantial potential in applications such as lipid nanoparticle (LNP) and other nanomedicine formulations in the future. The insights and knowledge derived from this investigation offer fundamental guidance, which could facilitate the clinical translation of next-generation polymer-protein conjugates.

Ethics approval and consent to participate

All animal experiments were performed in compliance with the Guideline for the Care and Use of Laboratory Animals, and were approved by the Experimental Animal Ethics Committee in Beijing (NKYY-DWLL-2020; CCME-LH-2).

CRediT authorship contribution statement

Jialing Sun: Conceptualization, Data curation, Writing – original

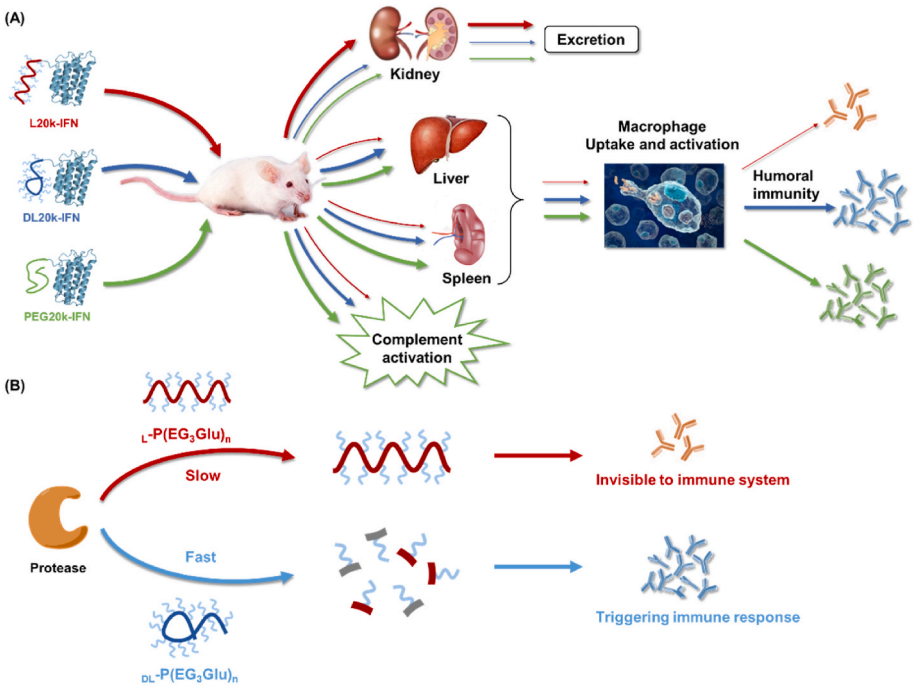

Fig. 8. (A) Schematic illustration of the different fates of L20k-IFN (red), DL20k-IFN (blue) and PEG20k-IFN (green) upon intravenous injection. (B) Schematic illustration of the different fates of L20k-IFN (red) and DL20k-IFN (blue) upon proteolysis. The three IFN conjugates are represented by arrows with different colors, and the varying widths of the arrows reflect the relative extents of organ distribution, cellular uptake, proteolytic breakdown, and/or elimination.

draft. **Junyi Chen:** Data curation, Formal analysis, Methodology. **Yiming Sun:** Data curation, Formal analysis. **Yingqin Hou:** Conceptualization. **Zhibo Liu:** Conceptualization, Project administration, Supervision. **Hua Lu:** Conceptualization, Formal analysis, Funding acquisition, Project administration, Writing – review & editing.

Declaration of competing interest

H.L. is a stockholder of a startup biotech company developing $_{L}$-P(EG_3Glu) and its use as a conjugation polymer for protein/peptide drugs.

Acknowledgement

This work is supported by the National Key Research and Development Program of China (2019YFA0904203), Beijing Natural Science Foundation Key Project (Z220023), and the National Natural Science Foundation of China (NSFC) for Distinguished Young Investigators (22125101).

Appendix A. Supplementary data

Supplementary data to this article can be found online at https://doi.org/10.1016/j.bioactmat.2023.10.011.

References

[1] G. Pasut, F.M. Veronese, State of the art in PEGylation: the great versatility achieved after forty years of research, J. Contr. Release 161 (2) (2012) 461–472.
[2] M.J. Bossard, M.J. Vicent, 2 - PEGylated proteins: a rational design for mitigating clearance mechanisms and altering biodistribution, in: G. Pasut, S. Zalipsky (Eds.), Polymer-Protein Conjugates, Elsevier, 2020, pp. 23–40.
[3] K. Knop, R. Hoogenboom, D. Fischer, U.S. Schubert, Poly(ethylene glycol) in drug delivery: pros and cons as well as potential alternatives, Angew. Chem., Int. Ed. 49 (36) (2010) 6288–6308.
[4] I. Ekladious, Y.L. Colson, M.W. Grinstaff, Polymer-drug conjugate therapeutics: advances, insights and prospects, Nat. Rev. Drug Discov. 18 (4) (2019) 273–294.
[5] A. Rudra, J. Li, R. Shakur, S. Bhagchandani, R. Langer, Trends in Therapeutic Conjugates: Bench to Clinic, Bioconjugate Chem. 31 (2020) 462–473.
[6] C. Chen, D.Y. Wah Ng, T. Weil, Polymer bioconjugates: modern design concepts toward precision hybrid materials, Prog. Polym. Sci. 105 (2020), 101241.
[7] E. Rohner, R. Yang, K.S. Foo, A. Goedel, K.R. Chien, Unlocking the promise of mRNA therapeutics, Nat. Biotechnol. 40 (11) (2022) 1586–1600.
[8] H. Schellekens, W.E. Hennink, V. Brinks, The immunogenicity of polyethylene glycol: facts and fiction, Pharmaceut. Res. 30 (7) (2013) 1729–1734.
[9] N.E. Elsadek, A.S. Abu Lila, T. Ishida, 5 - immunological responses to PEGylated proteins: anti-PEG antibodies, in: G. Pasut, S. Zalipsky (Eds.), Polymer-Protein Conjugates, Elsevier, 2020, pp. 103–123.
[10] P. Zhang, F. Sun, S.J. Liu, S.Y. Jiang, Anti-PEG antibodies in the clinic: current issues and beyond PEGylation, J. Contr. Release 244 (2016) 184–193.
[11] P.L. Turecek, J. Siekmann, 4 - PEG–protein conjugates: nonclinical and clinical toxicity considerations, in: G. Pasut, S. Zalipsky (Eds.), Polymer-Protein Conjugates, Elsevier, 2020, pp. 61–101.
[12] P. Bigini, M. Gobbi, M. Bonati, A. Clavenna, M. Zucchetti, S. Garattini, G. Pasut, The role and impact of polyethylene glycol on anaphylactic reactions to COVID-19 nano-vaccines, Nat. Nanotechnol. (2021) 1169–1171.
[13] L. Xu, J.P. Yang, B. Xue, C. Zhang, L.L. Shi, C.W. Wu, Y. Su, X. Jin, Y.M. Liu, X. Y. Zhu, Molecular insights for the biological interactions between polyethylene glycol and cells, Biomaterials 147 (2017) 1–13.
[14] A.M. Fletcher, P. Tellier, J. Douville, P. Mansell, M.J. Graziano, R.S. Mangipudy, T. A. Brodie, W.E. Achanzar, Adverse vacuolation in multiple tissues in cynomolgus monkeys following repeat-dose administration of a PEGylated protein, Toxicol. Lett. 317 (2019) 120–129.
[15] K. Sroda, J. Rydlewski, M. Langner, A. Kozubek, M. Grzybek, A.F. Sikorski, Repeated injections of PEG-PE liposomes generate anti-PEG antibodies, Cell. Mol. Biol. Lett. 10 (1) (2005) 37–47.
[16] P. Sellaturay, S. Nasser, S. Islam, P. Gurugama, P.W. Ewan, Polyethylene glycol (PEG) is a cause of anaphylaxis to the Pfizer/BioNTech mRNA COVID-19 vaccine, Clin. Exp. Allergy 51 (6) (2021) 861–863.
[17] M.C. Castells, E.J. Phillips, Maintaining safety with SARS-CoV-2 vaccines, N. Engl. J. Med. 384 (7) (2021) 643–649.
[18] T.J. Povsic, M.G. Lawrence, A.M. Lincoff, R. Mehran, C.P. Rusconi, S. L. Zelenkofske, Z. Huang, J. Sailstad, P.W. Armstrong, P.G. Steg, C. Bode, R. C. Becker, J.H. Alexander, N.F. Adkinson, A.I. Levinson, R.-P. Investigators, Pre-existing anti-PEG antibodies are associated with severe immediate allergic reactions to pegnivacogin, a PEGylated aptamer, J. Allergy Clin. Immunol. 138 (6) (2016) 1712–1715.
[19] K.U. Eckardt, ANAEMIA the safety and efficacy of peginesatide in patients with CKD, Nat. Rev. Nephrol. 9 (4) (2013) 192–193.
[20] A.S. Abu Lila, H. Kiwada, T. Ishida, The accelerated blood clearance (ABC) phenomenon: clinical challenge and approaches to manage, J. Contr. Release 172 (1) (2013) 38–47.
[21] S.E. Emam, N.E. Elsadek, A.S. Abu Lila, H. Takata, Y. Kawaguchi, T. Shimizu, H. Ando, Y. Ishima, T. Ishida, Anti-PEG IgM production and accelerated blood clearance phenomenon after the administration of PEGylated exosomes in mice, J. Contr. Release : official journal of the Controlled Release Society 334 (2021) 327–334.

[22] X.Y. Wang, T. Ishida, H. Kiwada, Anti-PEG IgM elicited by injection of liposomes is involved in the enhanced blood clearance of a subsequent dose of PEGylated liposomes, J. Contr. Release 119 (2) (2007) 236–244.
[23] E.T.M. Dams, P. Laverman, W.J.G. Oyen, G. Storm, G.L. Scherphof, J.W.M. Van der Meer, F.H.M. Corstens, O.C. Boerman, Accelerated blood clearance and altered biodistribution of repeated injections of sterically stabilized liposomes, J. Pharmacol. Exp. Therapeut. 292 (3) (2000) 1071–1079.
[24] P.E. Lipsky, L.H. Calabrese, A. Kavanaugh, J.S. Sundy, D. Wright, M. Wolfson, M. A. Becker, Pegloticase immunogenicity: the relationship between efficacy and antibody development in patients treated for refractory chronic gout, Arthritis Res. Ther. 16 (2) (2014) R60.
[25] P. Zhang, F. Sun, H.C. Hung, P. Jain, K.J. Leger, S.Y. Jiang, Sensitive and quantitative detection of anti-poly(ethylene glycol) (PEG) antibodies by methoxy-PEG-coated surface plasmon resonance sensors, Anal. Chem. 89 (16) (2017) 8217–8222.
[26] Y. Ju, W.S. Lee, E.H. Pilkington, H.G. Kelly, S.Y. Li, K.J. Selva, K.M. Wragg, K. Subbarao, T.H.O. Nguyen, L.C. Rowntree, L.F. Allen, K. Bond, D.A. Williamson, N.P. Truong, M. Plebanski, K. Kedzierska, S. Mahanty, A.W. Chung, F. Caruso, A. K. Wheatley, J.A. Juno, S.J. Kent, Anti-PEG antibodies boosted in humans by SARS-CoV-2 lipid nanoparticle mRNA vaccine, ACS Nano 16 (8) (2022) 11769–11780.
[27] J.H. Ko, H.D. Maynard, A guide to maximizing the therapeutic potential of protein-polymer conjugates by rational design, Chem. Soc. Rev. 47 (24) (2018) 8998–9014.
[28] E.M. Pelegri-O'Day, E.W. Lin, H.D. Maynard, Therapeutic protein-polymer conjugates: advancing beyond PEGylation, J. Am. Chem. Soc. 136 (41) (2014) 14323–14332.
[29] B.W. Li, P. Jain, J.R. Ma, J.K. Smith, Z.F. Yuan, H.C. Hung, Y.W. He, X.J. Lin, K. Wu, J. Pfaendtner, S.Y. Jiang, Trimethylamine N-oxide-derived zwitterionic polymers: a new class of ultralow fouling bioinspired materials, Sci. Adv. 5 (6) (2019) eaaw9562.
[30] P. Zhang, P. Jain, C. Tsao, Z. Yuan, W. Li, B. Li, K. Wu, H.C. Hung, X. Lin, S. Jiang, Polypeptides with high zwitterion density for safe and effective therapeutics, Angew. Chem., Int. Ed. 57 (26) (2018) 7743–7747.
[31] Y.Z. Qi, A. Simakova, N.J. Ganson, X.H. Li, K.M. Luginbuhl, I. Ozer, W.G. Liu, M. S. Hershfield, K. Matyjaszewski, A. Chilkoti, A brush-polymer/exendin-4 conjugate reduces blood glucose levels for up to five days and eliminates poly(ethylene glycol) antigenicity, Nat. Biomed. Eng. 1 (1) (2017), 0002.
[32] H. Frey, R. Haag, Dendritic polyglycerol: a new versatile biocompatible-material, J. Biotechnol. 90 (3–4) (2002) 257–267.
[33] S. Schottler, G. Becker, S. Winzen, T. Steinbach, K. Mohr, K. Landfester, V. Mailander, F.R. Wurm, Protein adsorption is required for stealth effect of poly (ethylene glycol)- and poly(phosphoester)-coated nanocarriers, Nat. Nanotechnol. 11 (4) (2016) 372–377.
[34] S.S. Nogueira, A. Schlegel, K. Maxeiner, B. Weber, M. Barz, M.A. Schroer, C. E. Blanchet, D.I. Svergun, S. Ramishetti, D. Peer, P. Langguth, U. Sahin, H. Haas, Polysarcosine-functionalized lipid nanoparticles for therapeutic mRNA delivery, ACS Appl. Nano Mater. 3 (11) (2020) 10634–10645.
[35] Y. Hu, Y. Hou, H. Wang, H. Lu, Polysarcosine as an alternative to PEG for therapeutic protein conjugation, Bioconjugate Chem. 29 (7) (2018) 2232–2238.
[36] M. Liu, P. Johansen, F. Zabel, J.C. Leroux, M.A. Gauthier, Semi-permeable coatings fabricated from comb-polymers efficiently protect proteins *in vivo*, Nat. Commun. 5 (2014) 5526.
[37] M. Dirauf, C. Grune, C. Weber, U.S. Schubert, D. Fischer, Poly(ethylene glycol) or poly(2-ethyl-2-oxazoline) – a systematic comparison of PLGA nanoparticles from the bottom up, Eur. Polym. J. 134 (2020).
[38] I. Ozer, G.A. Pitoc, J.M. Layzer, A. Moreno, L.B. Olson, K.D. Layzer, A.M. Hucknall, B.A. Sullenger, A. Chilkoti, PEG-Like brush polymer conjugate of RNA aptamer that shows reversible anticoagulant activity and minimal immune response, Adv. Mater. 34 (10) (2022) 2107852.
[39] M. Schlapschy, U. Binder, C. Borger, I. Theobald, K. Wachinger, S. Kisling, D. Haller, A. Skerra, PASylation: a biological alternative to PEGylation for extending the plasma half-life of pharmaceutically active proteins, Protein Eng. Des. Sel. 26 (8) (2013) 489–501.
[40] V. Schellenberger, C.W. Wang, N.C. Geething, B.J. Spink, A. Campbell, W. To, M. D. Scholle, Y. Yin, Y. Yao, O. Bogin, J.L. Cleland, J. Silverman, W.P.C. Stemmer, A recombinant polypeptide extends the in vivo half-life of peptides and proteins in a tunable manner, Nat. Biotechnol. 27 (12) (2009) 1186–1190.
[41] J. Hu, G.L. Wang, X.Y. Liu, W.P. Gao, Enhancing pharmacokinetics, tumor accumulation, and antitumor efficacy by elastin-like polypeptide fusion of interferon alpha, Adv. Mater. 27 (45) (2015) 7320–7324.
[42] Y. Yu, W.Z. Xu, X.M. Huang, X. Xu, R.R. Qiao, Y.H. Li, F. Han, H. Peng, T.P. Davis, C.K. Fu, A.K. Whittaker, Proteins conjugated with sulfoxide-containing polymers show reduced macrophage cellular uptake and improved pharmacokinetics, ACS Macro Lett. 9 (6) (2020) 799–805.
[43] X. Xu, X.M. Huang, Y.X. Chang, Y. Yu, J.C. Zhao, N. Isahak, J.S. Teng, R.R. Quo, H. Peng, C.X. Zhao, T.P. Davis, C.K. Fu, A.K. Whittaker, Antifouling surfaces enabled by surface grafting of highly hydrophilic sulfoxide polymer brushes, Biomacromolecules 22 (2) (2021) 330–339.
[44] C.K. Fu, B. Demir, S. Alcantara, V. Kumar, F. Han, H.G. Kelly, X. Tan, Y. Yu, W. Z. Xu, J.C. Zhao, C. Zhang, H. Peng, C. Boyer, T.M. Woodruff, S.J. Kent, D. J. Searles, A.K. Whittaker, Low-Fouling fluoropolymers for bioconjugation and in vivo tracking, Angew. Chem., Int. Ed. 59 (12) (2020) 4729–4735.
[45] A.J. Russell, S.L. Baker, C.M. Colina, C.A. Figg, J.L. Kaar, K. Matyjaszewski, A. Simakova, B.S. Sumerlin, Next generation protein-polymer conjugates, AIChE J. 64 (9) (2018) 3230–3245.
[46] Y. Tian, Z. Gao, N. Wang, M. Hu, Y. Ju, Q. Li, F. Caruso, J. Hao, J. Cui, Engineering poly(ethylene glycol) nanoparticles for accelerated blood clearance inhibition and targeted drug delivery, J. Am. Chem. Soc. 144 (40) (2022) 18419–18428.
[47] R. d'Arcy, F. El Mohtadi, N. Francini, C.R. DeJulius, H. Back, A. Gennari, M. Geven, M. Lopez-Cavestany, Z.Y. Turhan, F. Yu, J.B. Lee, M.R. King, L. Kagan, C.L. Duvall, N. Tirelli, A reactive oxygen species-scavenging 'stealth' polymer, poly (thioglycidyl glycerol), outperforms poly(ethylene glycol) in protein conjugates and nanocarriers and enhances protein stability to environmental and biological stressors, J. Am. Chem. Soc. 144 (46) (2022) 21304–21317.
[48] S. Liang, Y. Liu, X. Jin, G. Liu, J. Wen, L.L. Zhang, J. Li, X.B. Yuan, I.S.Y. Chen, W. Chen, H. Wang, L.Q. Shi, X.Y. Zhu, Y.F. Lu, Phosphorylcholine polymer nanocapsules prolong the circulation time and reduce the immunogenicity of therapeutic proteins, Nano Res. 9 (4) (2016) 1022–1031.
[49] T.J. Deming, Synthetic polypeptides for biomedical applications, Prog. Polym. Sci. 32 (8–9) (2007) 858–875.
[50] H. Lu, J. Wang, Z. Song, L. Yin, Y. Zhang, H. Tang, C. Tu, Y. Lin, J. Cheng, Recent advances in amino acid *N*-carboxyanhydrides and synthetic polypeptides: chemistry, self-assembly and biological applications, Chem. Commum. 50 (2) (2014) 139–155.
[51] A. Rasines Mazo, S. Allison-Logan, F. Karimi, N.J. Chan, W. Qiu, W. Duan, N. M. O'Brien-Simpson, G.G. Qiao, Ring opening polymerization of alpha-amino acids: advances in synthesis, architecture and applications of polypeptides and their hybrids, Chem. Soc. Rev. 49 (14) (2020) 4737–4834.
[52] Z. Song, H. Fu, R. Wang, L.A. Pacheco, X. Wang, Y. Lin, J. Cheng, Secondary structures in synthetic polypeptides from *N*-carboxyanhydrides: design, modulation, association, and material applications, Chem. Soc. Rev. 47 (19) (2018) 7401–7425.
[53] C. Bonduelle, Secondary structures of synthetic polypeptide polymers, Polym. Chem. 9 (13) (2018) 1517–1529.
[54] M. Yang, Z.-C. Zhang, F.-Z. Yuan, R.-H. Deng, X. Yan, F.-B. Mao, Y.-R. Chen, H. Lu, J.-K. Yu, An immunomodulatory polypeptide hydrogel for osteochondral defect repair, Bioact. Mater. 19 (2023) 678–689.
[55] C. Zhang, H. Lu, Helical nonfouling polypeptides for biomedical applications, chin, J. Polym. Sci. 40 (5) (2022) 433–446.
[56] Y. Hu, Z.-Y. Tian, W. Xiong, D. Wang, R. Zhao, Y. Xie, Y.-Q. Song, J. Zhu, H. Lu, Water-assisted and protein-initiated fast and controlled ring-opening polymerization of proline *N*-carboxyanhydride, Natl. Sci. Rev. 9 (8) (2022) nwac033.
[57] C. Dong, G.Q. Wu, C. Chen, X. Li, R. Yuan, L. Xu, H. Guo, J. Zhang, H. Lu, F. Wang, Site-specific conjugation of a selenopolypeptide to alpha-1-antitrypsin enhances oxidation resistance and pharmacological properties, Angew. Chem., Int. Ed. 61 (6) (2022), e202115241.
[58] Y. Hu, D. Wang, H. Wang, R. Zhao, Y. Wang, Y. Shi, J. Zhu, Y. Xie, Y.-Q. Song, H. Lu, An urchin-like helical polypeptide-asparaginase conjugate with mitigated immunogenicity, Biomaterials 268 (2021), 120606.
[59] H. Wang, Y. Hou, Y. Hu, J. Dou, Y. Shen, Y. Wang, H. Lu, Enzyme-activatable interferon–poly(α-amino acid) conjugates for tumor microenvironment potentiation, Biomacromolecules 20 (8) (2019) 3000–3008.
[60] Y. Hou, Y. Zhou, H. Wang, J. Sun, R. Wang, K. Sheng, J. Yuan, Y. Hu, Y. Chao, Z. Liu, H. Lu, Therapeutic protein PEPylation: the helix of nonfouling synthetic polypeptides minimizes antidrug antibody generation, ACS Cent. Sci. 5 (2) (2019) 229–236.
[61] Y. Hou, H. Lu, Protein PEPylation: a new paradigm of protein–polymer conjugation, Bioconjugate Chem. 30 (6) (2019) 1604–1616.
[62] C. Zhang, J. Yuan, J. Lu, Y. Hou, W. Xiong, H. Lu, From neutral to zwitterionic poly (alpha-amino acid) nonfouling surfaces: effects of helical conformation and anchoring orientation, Biomaterials 178 (2018) 728–737.
[63] Y. Hou, Y. Zhou, H. Wang, R. Wang, J. Yuan, Y. Hu, K. Sheng, J. Feng, S. Yang, H. Lu, Macrocyclization of interferon-poly(alpha-amino acid) conjugates significantly improves the tumor retention, penetration, and antitumor efficacy, J. Am. Chem. Soc. 140 (3) (2018) 1170–1178.
[64] Y. Hou, J. Yuan, Y. Zhou, J. Yu, H. Lu, A concise approach to site-specific topological protein-poly(amino acid) conjugates enabled by in-situ generated functionalities, J. Am. Chem. Soc. 138 (34) (2016) 10995–11000.
[65] Z. Shen, Y. Sun, G. Zhu, G. Xu, Z. Yu, H. Lu, Y. Chen, Molecular insights into the improved bioactivity of interferon conjugates attached to a helical polyglutamate, Langmuir 39 (18) (2023) 6539–6547.
[66] P.H. Maurer, Antigenicity of polypeptides (poly alpha amino acids) .10. Studies with polymers of D amino acids, Proc. Soc. Exp. Biol. Med. 113 (3) (1963) 553–557.
[67] P.H. Maurer, Antigenicity of polypeptides (Poly-Alpha-Amino acids) .17. Immunologic studies in humans with polymers containing L or D and L-alpha-amino acids, J. Immunol. 95 (6) (1965) 1095–1099.
[68] J.R. Uren, R.C. Ragin, Improvement in the therapeutic, immunological, and clearance properties of escherichia-coli and erwinia-carotovora L-asparaginases by attachment of poly-dl-alanyl peptides, Cancer Res. 39 (6) (1979) 1927–1933.
[69] H.J. Sage, G.F. Deutsch, G.D. Fasman, L. Levine, The serological specificity of the poly-alanine immune system, Immunochemistry 1 (2) (1964) 133–144.
[70] D.H. Zhang, Q. Chen, Y.F. Bi, H.D. Zhang, M.Z. Chen, J.L. Wan, C. Shi, W.J. Zhang, J.Y. Zhang, Z.Q. Qiao, J. Li, S.F. Chen, R.H. Liu, Bio-inspired poly-DL-serine materials resist the foreign-body response, Nat. Commun. 12 (1) (2021) 5327.
[71] C.J. White, J.W. Bode, PEGylation and dimerization of expressed proteins under near equimolar conditions with potassium 2-pyridyl acyltrifluoroborates, ACS Cent. Sci. 4 (2) (2018) 197–206.

[72] J. Yuan, Y. Sun, J. Wang, H. Lu, Phenyl trimethylsilyl sulfide-mediated controlled ring-opening polymerization of alpha-amino acid *N*-carboxyanhydrides, Biomacromolecules 17 (3) (2016) 891–896.
[73] J. Yuan, Y. Zhang, Z. Li, Y. Wang, H. Lu, A S-Sn lewis pair-mediated ring-opening polymerization of α-amino acid *N*-carboxyanhydrides: fast kinetics, high molecular weight, and facile bioconjugation, ACS Macro Lett. 7 (8) (2018) 892–897.
[74] A. Moreno, G.A. Pitoc, N.J. Ganson, J.M. Layzer, M.S. Hershfield, A.F. Tarantal, B. A. Sullenger, Anti-PEG antibodies inhibit the anticoagulant activity of PEGylated aptamers, Cell Chem. Biol. 26 (5) (2019) 634–644.
[75] Krystexxatm (Pegloticase) for Intravenous Infusion, Food and Drug Administration, 2009.
[76] J.S. Sundy, N.J. Ganson, S.J. Kelly, E.L. Scarlett, C.D. Rehrig, W. Huang, M. S. Hershfield, Pharmacokinetics and pharmacodynamics of intravenous PEGylated recombinant mammalian urate oxidase in patients with refractory gout, Arthritis Rheum-Us 56 (3) (2007) 1021–1028.
[77] Y. Mima, Y. Hashimoto, T. Shimizu, H. Kiwada, T. Ishida, Anti-PEG IgM is a major contributor to the accelerated blood clearance of polyethylene glycol-conjugated protein, Mol. Pharm. 12 (7) (2015) 2429–2435.
[78] W.-A. Chen, D.-Y. Chang, B.-M. Chen, Y.-C. Lin, Y. Barenholz, S.R. Roffler, Antibodies against poly(ethylene glycol) activate innate immune cells and induce hypersensitivity reactions to PEGylated nanomedicines, ACS Nano 17 (6) (2023) 5757–5772.
[79] P.H. Maurer, Antigenicity of polypeptides (poly alpha amino acids) .13. Immunological studies with synthetic polymers containing only D- or D- and L-alpha-amino acids, J. Exp. Med. 121 (3) (1965) 339-349.